Influence of finite size effects on exchange anisotropy in oxidized Co nanocluster assembled films

A. N. Dobrynin, D. N. Ievlev, C. Hendrich, K. Temst, and P. Lievens*
Laboratorium voor Vaste-Stoffysica en Magnetisme and Institute for Nanoscale Physics and Chemistry, K. U. Leuven, Celestijnenlaan 200D, B-3001 Leuven, Belgium

U. Hörmann, J. Verbeeck, and G. Van Tendeloo
Elektronenmicroscopie voor Materiaalonderzoek, Universiteit Antwerpen, Groenenborgerlaan 171, B-2020 Antwerp, Belgium

A. Vantomme
Instituut voor Kern- en Stralingsfysica and Institute for Nanoscale Physics and Chemistry, K.U.Leuven, Celestijnenlaan 200D, B-3001 Leuven, Belgium

(Received 2 December 2005; revised manuscript received 28 April 2006; published 15 June 2006)

We compare the magnetic properties of Co cluster assembled films with different degrees of oxidation. Clusters with grain size (2.3 ± 0.7) nm are produced in a laser vaporization cluster source and soft-landed in ultrahigh vacuum conditions, forming highly porous nanogranular films. After exposure to air for different periods of time, the Co clusters oxidize and the sample may be considered as a thin antiferromagnetic Co oxide matrix containing ferromagnetic Co clusters. Magnetization measurements were performed in a temperature range from 300 down to 5 K, at applied magnetic fields up to 30 kOe. The exchange bias value at 5 K for the strongly oxidized sample is 4.8 kOe against the value of 0.75 kOe for the less oxidized sample. The mean values of the thicknesses of the Co oxide layers are estimated to be 0.6 and 0.3 nm for the more and less oxidized sample, respectively. We propose a method of measuring the exchange bias inducing temperature, i.e., the temperature at which exchange anisotropy is established. We determined the mean inducing temperatures for both samples, which are 55 and 25 K, respectively, for the more and less oxidized samples. Both temperatures are well below the bulk CoO Néel temperature of 292 K. A low value of the inducing temperature of the Co oxide layer is a consequence of its subnanometer thickness, while a large exchange bias value is a consequence of different dimensionality of Co clusters and Co oxide matrix.

DOI: 10.1103/PhysRevB.73.245416 PACS number(s): 75.30.Et, 75.50.Ee, 75.50.Tt, 75.70.Cn

I. INTRODUCTION

Magnetic systems with reduced dimensionality, such as two-dimensional thin layers, one-dimensional nanowires, or zero-dimensional nanoparticles, show properties different from the bulk materials due to finite-size effects. In particular, magnetic ordering temperature and magnetocrystalline anisotropy were shown to be size dependent in many materials.[1–5] The reason for such behavior is a reduced coordination number, and a matching of the systems' characteristic size to a relevant physical length, such as the exchange correlation length and magnetic domain wall thickness. We investigate the influence of finite-size effects in oxidized Co nanocluster assembled films on the magnetic exchange anisotropy.

A unidirectional exchange anisotropy appears in hybrid ferromagnetic- (FM-) antiferromagnetic (AFM) systems when cooling down in an applied magnetic field through the Néel temperature of the antiferromagnet.[6] This leads to the AFM part adopting a spin structure, which minimizes the AFM-FM interfacial interaction (e.g., with AFM spins parallel to the FM spins at the interface). When applying a magnetic field with the opposite sign, the AFM part remains mostly unchanged (unless the external field is higher than the spin-flop transition field of the antiferromagnet), while the FM part is reversing, thus minimizing its energy. In addition to the ferromagnet's own anisotropy (magnetocrystalline, magnetoelastic and shape), an exchange interaction at the FM-AFM interface leads to an additional anisotropy, when it is easier to reverse the FM spins in the cooling field direction, than in the opposite one. This leads to a shift of the magnetic hysteresis loop along the field axis, named exchange bias.[6–11] This effect is used in spin valves, and it is promising for overcoming the superparamagnetic limit in recording media.[12] The fundamental interest is in mechanisms of the exchange coupling at the FM-AFM interface. By now, it seems that there are a number of mechanisms that could explain exchange bias, such as spin-flop coupling,[13,14] hybrid domain walls,[15] and uncompensated AFM spins at the FM-AFM interface. The latter was shown to be the reason for exchange bias in many cases, and in particular in Co/CoO systems.[16,17] The first direct observation of an interfacial net moment in the antiferromagnet was provided by Hoffman *et al.*,[18] and investigated in detail for various FM-AFM systems by Roy *et al.*[19]

It is known that a reduction of the AFM layer thickness in FM-AFM bilayers leads to the disappearance of the exchange bias effect at a certain point.[20] More recently, it was shown that the total AFM anisotropy energy, rather than the AFM layer thickness, determines whether exchange bias does appear.[21] For the isolated FM-AFM nanoparticle there is a critical size below which the exchange bias cannot be realized for any ratio of FM to AFM parts in the particle, due to the dominant role of the area-proportional exchange interaction energy at the FM-AFM interface over other volume-related energies in the system.[22]

In this work we focus on the investigation of the influence of finite-size effects on the magnetic properties of cluster-

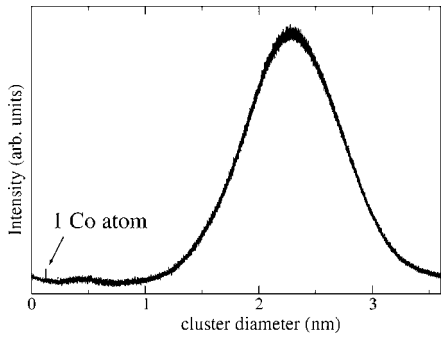

FIG. 1. Time of flight spectrum of Co clusters, used to grow the samples. The size spectrum is obtained from the directly measured mass spectrum approximating the cluster shape by spheres (see text for details).

assembled hybrid FM-AFM nanosystems. For this purpose we produced Co cluster films by the low energy cluster beam deposition technique.[23–26] Thus deposited clusters are in the size range 1–3 nm, and form highly porous films which, after exposure to air, form a thin AFM CoO matrix (two dimensional) with embedded FM Co clusters (zero dimensional).

II. SAMPLE PREPARATION AND CHARACTERIZATION

A. Low energy cluster beam deposition

The clusters were prepared in a laser vaporization source, described in detail elsewhere.[27–29] The laser beam [Nd:YAG, second harmonic (532 nm), Q-switched, pulse width=7 ns, E=150 mJ per pulse] is focused into a 1 mm^2 spot at the scanning Co target. The plasma is ablated into a cylindrical cavity (3 mm diameter, 20 mm length), where it is cooled with an ultra pure He (99.998%) gas pulse of 200 μs length, under a pressure of 8 bar. At the end of the cavity there is a 0.8 mm outlet, followed by a conical nozzle, where the clusters are supersonically expanded and further cooled. The cluster size distribution is monitored with a reflectron type time-of-flight (TOF) mass-spectrometer (MS), equipped with a dual microchannel plate detector. The typical cluster size distribution is shown in Fig. 1. The cluster size is obtained from the cluster mass (measured by TOF), using the following formula $d=2R_W N^{1/3}$, where R_W is the Wigner-Seitz radius (0.1383 nm for bulk Co), and N the number of atoms in the cluster. The TOF-MS resolution is decreasing with increasing mass, such that heavy clusters may not be resolved, and the overlapping peaks are observed as a "hump" in the TOF mass spectrum. This "hump" reflects the mass distribution of the produced clusters. The size distribution is relatively narrow (2.3±0.7 nm), and there are almost no small clusters produced. The one-atom peak indicated in Fig. 1 has a low intensity compared to the "hump" intensity. Taking into account that the amount of material is proportional to the area covered by the peak in the TOF spectrum,[29] the one-atom contribution in the cluster beam is negligible.

The cluster beam velocity is about 500 m/s, which corresponds to an energy of 0.07 eV per single Co atom, thus satisfying the conditions for low energy deposition.[30] The

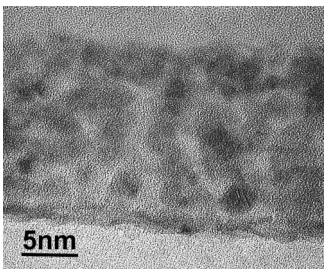

FIG. 2. The HRTEM micrograph shows a part of the layer in cross section geometry. The overview shows clearly that the film is highly porous, and consists of nanoparticles with a mean size about 2 nm.

clusters are deposited in an ultrahigh vacuum chamber (base pressure 10^{-10} mbar) onto 1 mm thick Si(100) substrates, covered with 700 nm of amorphous SiO_2. Since the deposition conditions are nondestructive, the clusters keep their structure, resulting in a highly-porous film. The deposition time for each sample was 1 h. After exposure to air the cluster surfaces are oxidized, that way forming a CoO matrix with embedded Co clusters. In this work we compare two samples with a different degree of oxidation. The first one (sample 1) was exposed to air for about 1 h before the measurements, while the second one (sample 2) was exposed to air for 1 h after each 20 min of deposition. Thus the expected ratio of Co oxide to Co is higher in sample 2 compared to sample 1.

B. Transmission electron microscopy and electron energy loss spectroscopy

We investigated cross sections of sample 1 and sample 2 by high resolution transmission electron microscopy (HRTEM) using a Jeol 4000EX operating at 400 kV with a point-resolution of 0.17 nm. The cross-section samples were prepared for HRTEM on a copper ring by the standard preparation technique using mechanical grinding and ion milling. During the mechanical grinding the samples are exposed to water which could cause additional oxidation of the Co particles. The layers were found to be smooth and had an average thickness of 15–20 nm, see Fig. 2. Figure 3 shows a

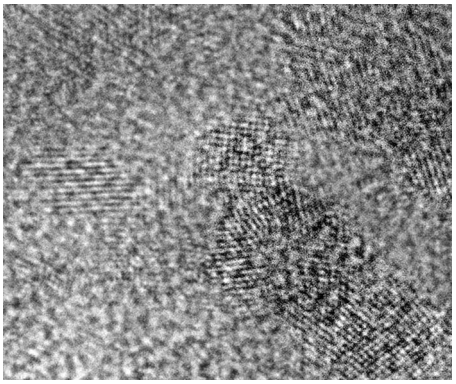

FIG. 3. The HRTEM micrograph shows a group of particles. The central particle has a diameter of 2 nm.

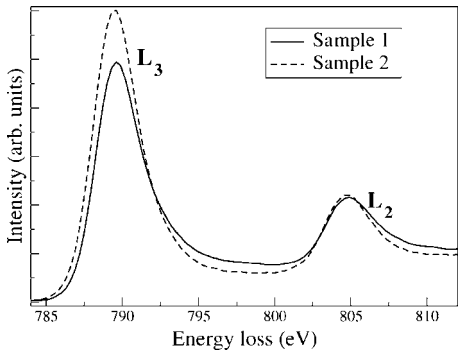

FIG. 4. EELS spectra from samples 1 and 2. The L_3/L_2 intensity ratio is systematically lower for the less oxidized sample.

HRTEM image of a group of clusters. The mean particle size is about 2–2.5 nm, which corresponds well to the value obtained by TOF-MS. The layer is highly porous, i.e., most of the Co particles are separated from each other, see Fig. 2.

Electron energy loss spectroscopy (EELS) experiments were carried out on a Jeol 3000F FEG-STEM equipped with a GIF 2000 post-column electron energy loss spectrometer. The microscope has a minimum probe diameter of 0.38 nm and an energy spread of 1.5 eV. For the EELS measurements we used plan view samples which are directly produced on TEM grids in the following way. First, a thin MgO layer was grown on NaCl(100) single crystal substrates. After that the NaCl was dissolved in distilled water and the thin MgO films were caught on copper TEM grids. Prior to deposition of the Co clusters the MgO layers were annealed for 1 h at 600 °C. Two samples, with production parameters identical to samples 1 and 2, were deposited on this substrate. The purpose of the EELS measurements was to demonstrate the different Co oxide content in the samples. The L_2 $(2p_{1/2})$ and L_3 $(2p_{3/2})$ absorption edges of Co were probed. These peaks correspond to $2p \rightarrow 3d$ transitions near the Fermi level. The intensities of the Co L_3 and L_2 edge resonances reflect the occurrence of vacancies in the d band. The L_3/L_2 intensity ratio is known to increase for regions with rising portions of oxidized Co, i.e., with a higher density of vacancies in the d band.[31]

Five spectra were taken from different positions on each sample. After background subtraction and removal of plural scattering effects by deconvolution, the intensities of the white lines were normalized in a 100 eV window starting 50 eV behind the L_3 edge onset. In Fig. 4 two spectra from samples 1 and 2 are compared. It is clear that there is a difference in the total white line intensity of the two samples. The intensity of the L_3 peak is lower for sample 1 than for sample 2, indicating that there is a smaller number of unoccupied $3d$ states in sample 1, i.e., higher amount of unoxidized Co. When calculating the L_3/L_2 ratio according to the prescription in Leapman[32] we find that the L_3/L_2 ratio in sample 1 is lower than in sample 2. Leapman[32] has shown for numerous transition metals and their oxides that the L_3/L_2 ratio is less pronounced in the case of the pure metal. Thus, the intensity distribution of the white lines contains evidence that the ratio of pure Co to oxidized Co in sample 1 is higher than that in sample 2.

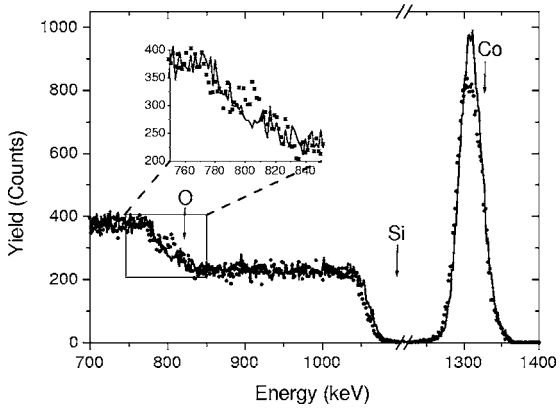

FIG. 5. ^{4}He backscattering spectra of the oxidized Co cluster sample 1 (solid line) and sample 2 (●), using a scattering angle of 105°. The arrows indicate the energy for scattering from, respectively, O, Si, and Co at the surface. The inset shows a zoom of the oxygen signal, clearly indicating the larger degree of oxidation (and hence the thicker layer) for sample 2.

C. Rutherford backscattering spectrometry

In order to determine the content of Co in the samples, Rutherford backscattering spectrometry experiments were performed using a 1.57 MeV $^4He^+$ beam. Two detectors were used, with a scattering angle of the detected particles of 12° and 75° for optimal quantification and optimal depth resolution, respectively. The RBS analysis was performed on several spots for each sample, resulting in a deviation of the mean areal Co density of less than 3% for sample 1 and 12% for sample 2. Moreover, within the experimental error, both samples contain the same amount of Co: an average Co thickness of 3.7×10^{16} atoms/cm^2 was obtained. This areal density corresponds to a Co layer thickness of approximately 4 nm, assuming the bulk atomic density of 8.97×10^{22} atoms/cm^2. Obviously, as a result of the porosity and the oxidation of the Co, the actual physical thickness of the layers is significantly larger, as inferred from the TEM analysis.

Due to the limited sensitivity of RBS to light elements, accurately quantifying the oxygen content in the layers is not readily possible. However, it is still possible to deduce qualitative information on the oxidation of the respective layers. From a comparison of the spectra (Fig. 5), it can be concluded that sample 2 contains significantly more oxygen than sample 1. First, the Co signal of sample 2 is lower and broader than the Co signal of sample 1 (resulting in the same area, i.e., the same Co areal density), indicating a thicker layer with a lower fraction of Co atoms, i.e., more oxidized. Secondly, the Si leading edge (around 1.05 MeV) has shifted towards a slightly lower energy in case of sample 2, indicating a thicker capping layer on top of the SiO_2 substrate, confirming the larger degree of oxidation for this sample. Thirdly, despite the poor sensitivity to oxygen, as described above, an increase in the oxygen signal is observed for sample 2 compared to sample 1 (see inset for a detailed view on the oxygen signal).

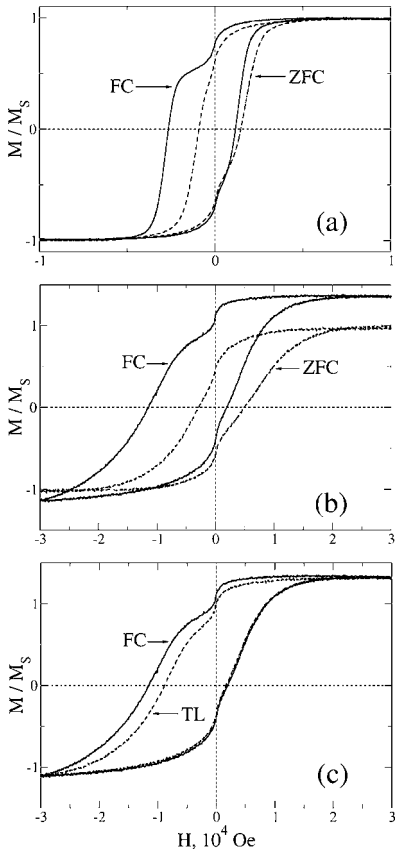

FIG. 6. Magnetic hysteresis loops, taken at 5 K, after ZFC and FC for sample 1 (a) and sample 2 (b). The ZFC was performed after magnetizing the sample until saturation at 300 K in the direction opposite to the direction of the external field in the FC case. (c) FC loop and training loop (TL) for sample 2.

III. MAGNETIZATION MEASUREMENTS

A. Field cooling and zero field cooling

In-plane magnetization versus field dependences were measured using a vibrating sample magnetometer in the temperature range from 5 to 300 K and in applied magnetic fields up to 30 kOe. In Fig. 6(a) zero field cooled (ZFC) and field cooled (FC) magnetic hysteresis loops for sample 1 are shown. The sample was cooled from 300 down to 5 K. The field cooling was performed in an applied magnetic field of 10 kOe. Before zero field cooling the sample was saturated (in a field of 100 Oe) in the direction opposite to the direction of the cooling field in the FC case. Such zero field cooling is in fact cooling in the remanent field of the FM part, which was recently shown to induce nonzero exchange bias.[33,34] The absolute value of the exchange bias after ZFC in the remanent state (H_Z=220 Oe) is lower than that after FC (H_F=750 Oe). In case of ZFC there was no difference in H_Z values for different saturating fields at 300 K (50 Oe, 100 Oe, 10 kOe). The direction of the bias is opposite to the cooling field (external in the FC case and remanent in the ZFC case) direction. The step in the upper part of the FC hysteresis loop shows the presence of a nonoxidized Co clusters part, which is not interacting much with the oxidized part of Co clusters. In this case the resulting loop is a superposition of the two independent hysteresis loops: one from pure Co clusters and another one from oxidized Co clusters.[35] Such behavior is typical for hybrid noninteracting and weakly interacting magnetic systems.[36]

In Fig. 6(b) the ZFC and FC hysteresis loops for sample 2 are shown. The FC and ZFC conditions were the same as for the first sample. The value of exchange bias for the ZFC H_Z=1000 Oe, and in the case of FC H_F=4800 Oe. While in the first sample there is no difference in magnetization saturation behavior for FC and ZFC, the second sample shows a significant vertical shift after field cooling in the first quarter of the hysteresis loop. This is not yet saturated in the third quarter, even by a field of 30 kOe. The reason for such vertical shift is the presence of strongly oxidized clusters, where the FM part is very small, and the AFM part is large, leading to pinning of the ferromagnet in the cooling field direction.[22] This effect is absent in the first sample, indicating that only slightly oxidized clusters are present there.

The field training effect[7,37,39] was observed for both samples after FC. In Fig. 6(c) the hysteresis loop after FC and the following loop (training loop) for sample 2 are compared. The third and the following hysteresis loops repeat the training loop in both samples. No training effect after ZFC in either sample was observed. The training effect was recently explained by the presence of several magnetic easy axes in an antiferromagnet.[37] While after FC the AFM spin sublattice is preferably oriented parallel to the cooling field, after the first field cycle it becomes energetically favorable for some AFM spins to orient along another easy axis. The exchange coupling between nonparallel FM and AFM spins is weaker than that for the parallel case, which leads to a lower exchange bias value.[37] Experimentally it was shown that applying a field perpendicular to the FC field at low temperatures leads to the reversing of the training effect in Co/CoO multilayers, thus proving the above described hypothesis.[39]

Since there was no training effect observed for both samples after ZFC, we can assume that an "optimal" AFM spin configuration is formed during the sample cooling, and no AFM spin sublattice reorientation happens after the field reversing. The training loop [Fig. 6(c)] is shifted more than the ZFC loop [Fig. 6(b)], which shows that there is an additional factor, which influences the lowest exchange bias value upon ZFC.

When ZFC, the magnetization vectors of the FM clusters are nonparallel to each other, as in the case of the FC. However, there is a preferential orientation of the FM magnetization vectors, which creates the remanent field. When passing the Néel temperature, a local AFM structure corresponding to the neighboring FM part is established, and the FM part is being pinned in its own direction. This direction determines the unidirectional anisotropy of this local FM-AFM part. In other words, this determines the easy direction of magnetization of the particular FM part. Thus, the preferential easy direction of magnetization of the whole sample coincides with the remanent field direction. The value of the exchange bias is reduced compared to the FC case, because a hard direction of one FM part in a sample is an easy direction for another one, etc.

Such nonparallel orientation of the FM magnetization vectors after ZFC may also lead to reducing the saturation

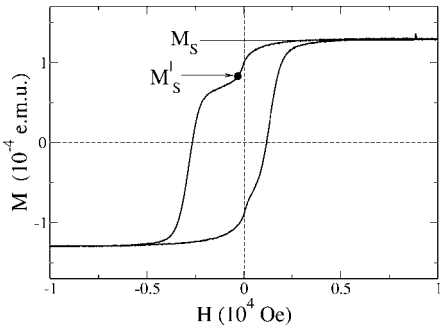

FIG. 7. FC hysteresis loop for sample 1. $M_S^{|}$: saturation magnetization of the oxidized Co clusters.

magnetization value in samples with strongly oxidized Co clusters. If the magnetization vectors of some FM parts are almost perpendicular to the external field, their Zeeman energy is very small, and the FM part stays pinned to the AFM part.[22]

B. Estimate of the CoO layer thickness

The thickness of the Co oxide layer may be estimated using the saturation magnetization value M_S and the amount of Co in each sample. In Fig. 7 the FC hysteresis loop for sample 1 is plotted, where $M_S=1.27\times10^{-4}$ e.m.u. The density of Co, σ, is obtained with RBS, and for both samples $\sigma=3.7\times10^{16}$ atoms/cm^2. The area of sample 1 is $S=32.8$ mm^2. The saturation magnetization of bulk fcc Co is $1.753\mu_B$/atom, or 1.62×10^{-20} e.m.u./atom. It was shown that Co clusters with more than 400–500 atoms (>1.5 nm) have the same magnetic moment per atom as bulk Co.[30] Therefore, if sample 1 would not be oxidized, its saturation magnetization value would be $M=1.94\times10^{-4}$ e.m.u. This way, the ratio $\alpha=M_S/M$ can be used to estimate the amount of FM Co in the sample, while the fraction of AFM CoO is equal to $(1-\alpha)$. For sample 1 there is a fraction $\alpha=0.65$ of pure Co, and $(1-\alpha)=0.35$ of CoO. For sample 2 $M_S=5\times10^{-5}$ e.m.u., $S=35.9$ mm^2, and the fraction of FM Co is 23%, while the fraction of CoO is 77%.

We must take into account that not all Co clusters in the samples are surrounded with CoO shells, as was discussed in Sec. III A. Since we observe a superposition of two independent hysteresis loops from nonoxidized and oxidized Co clusters (see Fig. 7), we can determine the value of magnetization $M_S^{|}$, at which the step in the hysteresis loop appears. The ratio $\gamma=M_S^{|}/M_S$ defines the ratio of oxidized Co clusters to all Co clusters in the sample. Therefore, the amount of cobalt in Co clusters that are surrounded with CoO shells is $N_{\text{core}}=\alpha\gamma N$, where N is the total amount of Co in the sample. The amount of Co in the AFM shells is $N_{\text{shell}}=(1-\alpha)N$. Assuming a perfect spherical Co-core, CoO-shell system with an external radius R and core radius r, one obtains

$$\left(\frac{R}{r}\right)^3 = 1 + \frac{\rho_{\text{Co}}}{\rho_{\text{CoO}}}\frac{m_{\text{CoO}}}{m_{\text{Co}}}\frac{1-\alpha}{\alpha\gamma}. \quad (1)$$

Here ρ_{Co}, ρ_{CoO} are densities and m_{Co}, m_{CoO} the molecular mass of Co and CoO, respectively. Although the density of Co and CoO in our samples may be different from their bulk values, we assume that the ratio of the densities $\rho_{\text{Co}}/\rho_{\text{CoO}}$ is the same as in the bulk. Then we get that for sample 1 $r=0.73R$, and for sample 2 $r=0.47R$. The thickness of the CoO matrix in the considered geometry is $d=R-r$. For a mean cluster size of 2.3 nm ($R=1.15$ nm) we obtain values for the CoO mean thickness of 0.3 nm for sample 1, and 0.6 nm for sample 2. We must stress that since the actual geometry may be different from perfect core-shell systems, these values are indicative only.

C. Exchange bias inducing temperature

It is "common knowledge" that a unidirectional exchange anisotropy is established when field cooling ferromagnetic-antiferromagnetic systems through the Néel temperature of the antiferromagnet. This means that the vector of the cooling field when passing the Néel temperature determines the easy direction of magnetization of the hybrid system, because it defines the orientation of the antiferromagnetic spin structure. In case of a zero ZFC exchange bias value this means that it is impossible to induce exchange bias if the external field is applied at temperatures lower than the Néel temperature of the antiferromagnet. If there is a nonzero ZFC (to be more precise, remanent field cooled) exchange bias value, as in our case, applying an external field at a value below the Néel temperature should not change the easy direction of magnetization.

However, for oxidized Co cluster films we are able to change the direction of exchange bias by applying the field at temperatures much lower than the Néel temperature of bulk CoO. This is especially surprising, since it was shown that the Néel temperature of an antiferromagnet is increasing in nanoscale ferromagnetic-antiferromagnetic systems, in comparison with the Néel temperature of a pure antiferromagnet.[4]

There may be two explanations for the observed behavior. The first one assumes that the Néel temperature of thin CoO shells is lower than the Néel temperature of bulk CoO due to finite-size effects. This is in agreement with many studies of thin antiferromagnetic films and nanoparticles (see, e.g., Refs. 3 and 38), but is contradicting the above mentioned enhancement of the Néel temperature in hybrid ferromagnetic-antiferromagnetic nanosystems. The second explanation is that it is not necessary to cool down a hybrid system from above the Néel temperature in order to induce exchange bias. The temperature from which the field cooling should be performed must be above the *inducing* temperature of exchange bias. This assumes that an interfacial antiferromagnetic spin structure (e.g., the orientation of uncompensated interfacial spins) can be changed above the inducing temperature, and it determines the easy direction of magnetization.

Independent of the nature of the inducing temperature, its mean value can be obtained experimentally. The following procedure for a measurement of the exchange bias inducing temperature was implemented. First, the sample is magnetized till saturation in the "negative" (opposite to the external field during FC) direction at a value above the Néel tempera-

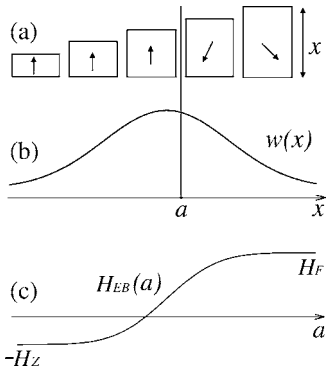

FIG. 8. (a) CoO shells of thickness x; the arrows indicate the easy direction of magnetization of the particular antiferromagnetic-ferromagnetic couple. (b) Probable distribution function of the CoO shells thickness $w(x)$. (c) Exchange bias as a function of CoO shell thickness a, to the inducing temperature of which the sample was zero field cooled.

ture of the bulk antiferromagnet. Then it is zero field cooled to the temperature T_{ind}, at which the "positive" magnetic field is applied, and the sample is further cooled down to the temperature at which the magnetization measurements are performed (in our case 5 K).

We assume that there is some distribution in Co oxide shell thickness x, which is changing from $x_{\min}$ to $x_{\max}$. Both blocking and Néel temperatures are functions of the antiferromagnetic layer thickness,[3] thus $T_{\mathrm{ind}}=T_{\mathrm{ind}}(x)$. A distribution function $w(x)$ can be introduced, such that $\int_{x_{\min}}^{x_{\max}} w(x)dx=1$. Figure 8(a) shows a schematic drawing of shells of different thickness; in Fig. 8(b) their probable distribution function is plotted. Therefore, when ZFC to the temperature $T_{\mathrm{ind}}(a)$, part of the CoO shells with $x>a$ will be in the blocked state, while those with $x<a$ are still in the unblocked state. Further FC leads to establishing the interfacial antiferromagnetic structure in the shells with $x<a$. The easy direction of magnetization for the shells with $x>a$ is determined by the remanent fields of their ferromagnetic Co cores. For the shells with $x<a$ the easy direction is determined by the cooling field. This situation is illustrated in Fig. 8(a), where arrows on the schematic shells are indicating the easy direction of magnetization of the particular ferromagnetic-antiferromagnetic couple. Here the cooling field direction is positive (up arrows), and the remanent field is negative (nonparallel down arrows). After field cooling to the measuring temperature (5 K), the part with $x<a$ contributes to the exchange bias value H_F, while the part with $x>a$ contributes to the exchange bias value $-H_Z$. If a constant size of the ferromagnetic cores is assumed, the general expression for the exchange bias as a function of a can be written as

$$H_{\mathrm{EB}}(a)=H_F\int_{x_{\min}}^{a} w(x)dx-H_Z\int_{a}^{x_{\max}} w(x)dx. \qquad (2)$$

Here $x,a\in[x_{\min};x_{\max}]$. This dependence is schematically drawn in Fig. 8(c). Expression (2) is illustrative only: in our samples the ferromagnetic core size is not uniform and also influenced by the cluster dependent degree of oxidation,

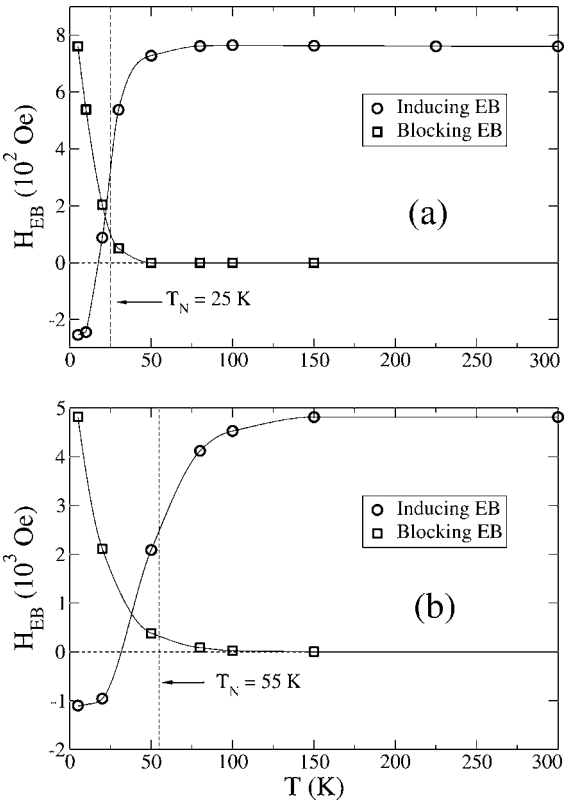

FIG. 9. Exchange bias inducing and blocking temperatures for sample 1 (a) and sample 2 (b). Lines are a guide to the eye.

which complicates any analytical description significantly. However, this simplified model still helps to understand the experimental data, as described below.

The dependence of the exchange bias value on the inducing temperature of a shell of thickness a can be obtained experimentally. For this purpose, the sample was magnetized until saturation in the "negative" direction in a field of 100 Oe at 300 K. Then it was zero field cooled to the temperature T_{ind}, at which a "positive" external field of 10 kOe was applied, and the sample was field cooled to 5 K. The dependence of the exchange bias on the inducing temperature is plotted in Fig. 9(a) for sample 1 and in Fig. 9(b) for sample 2 (circles, line is a guide to the eye). Both samples show a transition between their H_F and $-H_Z$ values of the exchange bias. The mean inducing temperature may be extracted from these experimental curves as

$$\langle T_{\mathrm{ind}}\rangle=\frac{1}{H_F+H_Z}\int_{-H_Z}^{H_F} T_{\mathrm{ind}}(H)dH. \qquad (3)$$

For sample 1 this value is 25 K, and for sample 2 $\langle T_{\mathrm{ind}}\rangle$ =55 K. Both values are well below the bulk CoO Néel temperature of 292 K.

The proposed technique resembles the technique of measuring the distribution of blocking temperature, reported by Soeya *et al.*[40] In that case the sample is first field cooled to a temperature at which the exchange bias value is measured, then warmed up to a probing temperature, from which it is field cooled in a field of the opposite direction. This way the

temperature at which the direction of exchange anisotropy can be changed is probed.

We measured the blocking temperature of exchange bias by finding out the maximal temperature at which exchange bias exists after cooling from above the Néel temperature.[7] In Fig. 9 the exchange bias values are plotted as a function of the temperature to which the samples were cooled down from 300 K at the field of 10^4 Oe, for samples 1 (a) and 2 (b), respectively. These curves are labeled with squares. The mean value of the blocking temperature may not be determined in the same way as the mean value of the inducing temperature [see Eq. (3)]. The reason is that the exchange bias value depends on temperature, as does the coercivity. This means that even for a very sharp distribution function of CoO shell thicknesses (e.g., δ function), the exchange bias value as a function of temperature is decreasing gradually. Therefore it is impossible to distinguish between the decrease of the bias value due to its own temperature dependence, and due to the fact that at the measurement temperature some part of the CoO shells is in a paramagnetic (or unblocked) state. However, it is clear from Fig. 9 that the maximal value of the blocking temperature fairly well corresponds to that of the inducing temperature.

IV. CONCLUSIONS

Cobalt clusters were produced in a laser vaporization cluster source and soft landed by low-energy cluster beam deposition onto amorphous SiO_2 substrates. Characterization of the samples with transmission electron microscopy shows that the films are highly porous, and that the clusters are spherical with a mean size of about 2.5 nm, thus corresponding well to that observed in beam with time-of-flight mass spectrometry. For the two samples considered, exposed to air for different periods of time, both EELS and RBS showed a difference in the degree of oxidation. Magnetization measurements revealed that the value of exchange bias for the strongly oxidized sample is about an order of magnitude higher than that for the slightly oxidized sample (4.8 kOe against 0.75 kOe). An estimate of the thickness of the Co oxide layer, based on combining magnetization and RBS data, yields 0.6 nm for the more oxidized sample and 0.3 nm for the less oxidized sample. In spite of the very low AFM matrix thickness, the exchange bias reaches high values. At first sight this seems to contradict the earlier observed vanishing of exchange bias in FM-AFM films with thin AFM layers,[20,21] and in systems of FM-core–AFM-shell nanoparticles.[22] In those systems the AFM anisotropy energy is lower than the interfacial exchange interaction and the Zeeman energies, which leads to the rotation of the AFM spins coherently with the FM spins. Both thin FM-AFM layers and core-shell nanoparticles are hybrid systems with equal dimensionality of the constituents: two dimensional in the first case and zero dimensional in the latter case. After oxidation the Co cluster assembled film forms a Co oxide matrix (thin layer, two dimensional) with embedded Co clusters (zero dimensional). The higher dimensionality of the AFM matrix results in a high anisotropy energy value of the antiferromagnet, which is always larger than the exchange energy at the FM-AFM interface. This is also the reason for the high exchange bias values, since large fields are needed in order to reach a Zeeman energy of a single Co cluster which is large enough to overcome the AFM anisotropy energy barrier.

We presented a technique to measure the exchange bias inducing temperature, i.e., the temperature from which it is possible to induce exchange bias by field cooling. Mean values of the inducing temperature were obtained for both samples, 55 and 25 K, respectively, for the more (0.6 nm of CoO) and less (0.3 nm of CoO) oxidized sample. Both values are well below the Néel temperature of bulk CoO. The nature of the inducing temperature depends on the mechanism of establishing the interfacial antiferromagnetic structure. If the antiferromagnet determines the orientation of the interfacial spin structure, then the inducing temperature is the Néel temperature of the antiferromagnet. If the magnetization of the ferromagnet is aligning the interfacial uncompensated antiferromagnetic spins, then the inducing temperature corresponds to the blocking temperature of exchange bias.

ACKNOWLEDGMENTS

This work was supported by the Fund for Scientific Research–Flanders (FWO), the Flemish Concerted Action (Grant No. GOA/2004/02), the Belgian Interuniversity Poles of Attraction (Grant No. IAP/P5/01), and the European Community's Human Potential NanoCluster (Grant No. HPRN-CT-2002-00328) programs.

*Electronic address: Peter.Lievens@fys.kuleuven.be

[1] R. Skomski, J. Phys.: Condens. Matter **15**, R841 (2003).
[2] M. Jamet, W. Wernsdorfer, C. Thirion, D. Mailly, V. Dupuis, P. Mélinon, and A. Pérez, Phys. Rev. Lett. **86**, 4676 (2001).
[3] T. Ambrose and C. L. Chien, Phys. Rev. Lett. **76**, 1743 (1996).
[4] P. J. van der Zaag, Y. Ijiri, J. A. Borchers, L. F. Feiner, R. M. Wolf, J. M. Gaines, R. W. Erwin, and M. A. Verheijen, Phys. Rev. Lett. **84**, 6102 (2000).
[5] R. H. Kodama, S. A. Makhlouf, and A. E. Berkowitz, Phys. Rev. Lett. **79**, 1393 (1997).
[6] W. H. Meiklejohn and C. P. Bean, Phys. Rev. **102**, 1413 (1956).
[7] J. Nogués and Ivan K. Schuller, J. Magn. Magn. Mater. **192**, 203 (1999).
[8] A. E. Berkowitz and K. Takano, J. Magn. Magn. Mater. **200**, 552 (1999).
[9] M. Kiwi, J. Magn. Magn. Mater. **234**, 584 (2001).
[10] J. Nogués, J. Sort, V. Langlais, V. Skumryev, S. Surinach, J. S. Munoz, and M. D. Baró, Phys. Rep. **422**, 65 (2005).
[11] J. Nogués, J. Sort, V. Langlais, S. Doppiu, B. Dieny, J. S. Munoz, S. Surinach, M. D. Baró, S. Stoyanov, and Y. Zhang, Int. J. Nanotechnol. **2**, 23 (2005).
[12] V. Skumryev, S. Stoyanov, Y. Zhang, G. Hadjipanayis, D. Givord,

and J. Nogués, Nature (London) **423**, 850 (2003).
[13] Y. Ijiri, J. A. Borchers, R. W. Erwin, S.-H. Lee, P. J. van der Zaag, and R. M. Wolf, Phys. Rev. Lett. **80**, 608 (1998).
[14] T. J. Moran and I. K. Schuller, J. Appl. Phys. **79**, 5109 (1996).
[15] C. L. Chien, V. S. Gornakov, V. I. Nikitenko, A. J. Shapiro, and R. D. Shull, Phys. Rev. B **68**, 014418 (2003).
[16] H. Ohldag, A. Scholl, F. Nolting, E. Arenholz, S. Maat, A. T. Young, M. Carey, and J. Stöhr, Phys. Rev. Lett. **91**, 017203 (2003).
[17] K. Takano, R. H. Kodama, A. E. Berkowitz, W. Cao, and G. Thomas, Phys. Rev. Lett. **79**, 1130 (1997).
[18] A. Hoffmann, J. W. Seo, M. R. Fitzsimmons, H. Siegwart, J. Fompeyrine, J.-P. Locquet, J. A. Dura, and C. F. Majkrzak, Phys. Rev. B **66**, 220406 (2002).
[19] S. Roy, M. R. Fitzsimmons, S. Park, M. Dorn, O. Petracic, Igor V. Roshchin, Zhi-Pan Li, X. Batlle, R. Morales, A. Misra, X. Zhang, K. Chesnel, J. B. Kortright, S. K. Sinha, and Ivan K. Schuller, Phys. Rev. Lett. **95**, 047201 (2005).
[20] W. H. Meiklejohn, J. Appl. Phys. **33**, 1328 (1962).
[21] M. S. Lund, W. A. A. Macedo, Kai Liu, J. Nogués, Ivan K. Schuller, and C. Leighton, Phys. Rev. B **66**, 054422 (2002).
[22] A. N. Dobrynin, D. N. Ievlev, K. Temst, P. Lievens, J. Margueritat, J. Gonzalo, C. N. Afonso, S. Q. Zhou, A. Vantomme, E. Piscopiello, and G. Van Tendeloo, Appl. Phys. Lett. **87**, 012501 (2005).
[23] H. Haberland, Z. Insepov, and M. Moseler, Phys. Rev. B **51**, 11061 (1995).
[24] A. Perez, P. Melinon, V. Dupuis, P. Jensen, B. Prevel, J. Tuaillon, L. Bardotti, C. Maret, M. Treilleux, M. Broyer, M. Pellarin, J. L. Vaille, B. Palpant, and J. Lerme, J. Phys. D: Applied Physics **30**, 709 (1997).
[25] C. Bréchignac, Ph. Cahuzac, F. Carlier, M. de Frutos, A. Masson, C. Mory, C. Colliex, and B. Yoon, Phys. Rev. B **57**, R2084 (1998).
[26] B. Pauwels, G. Van Tendeloo, E. Zhurkin, M. Hou, G. Verschoren, L. T. Kuhn, W. Bouwen, and P. Lievens, Phys. Rev. B **63**, 165406 (2001).
[27] W. Bouwen, P. Toen, F. Vanhoutte, S. Bouckaert, F. Despa, H. Weidele, R. E. Silverans, and P. Lievens, Rev. Sci. Instrum. **71**, 54 (2000).
[28] N. Vandamme, E. Janssens, F. Vanhoutte, P. Lievens, and C. Van Haesendonck, J. Phys.: Condens. Matter **15**, S2983 (2003).
[29] A. N. Dobrynin, D. N. Ievlev, G. Verschoren, J. Swerts, M. J. Van Bael, K. Temst, P. Lievens, S. Q. Zhou, A. Vantomme, E. Piscopiello, and G. Van Tendeloo, Phys. Rev. B **73**, 104421 (2006).
[30] C. Binns, Surf. Sci. Rep. **44**, 1 (2001).
[31] K. Yu-Zhang, D. Imhoff, Y. Leprince-Wang, E. Roy, S. M. Zhou, and C. L. Chien, Acta Mater. **51**, 1157 (2003).
[32] R. D. Leapman, L. A. Grunes, and P. L. Fejes, Phys. Rev. B **26**, 614 (1982).
[33] P. Miltényi, M. Gierlings, M. Bamming, U. May, G. Güntherodt, J. Nogués, and M. Gruyters, Appl. Phys. Lett. **75**, 2304 (1999).
[34] N. J. Gökemeijer, J. W. Cai, and C. L. Chien, Phys. Rev. B **60**, 3033 (1999).
[35] E. Popova, H. Loosvelt, M. Gierlings, L. H. A. Leunissen, R. Jonckheere, C. Van Haesendonck, and K. Temst, Eur. Phys. J. B **44**, 491 (2005).
[36] Eric E. Fullerton, J. S. Jiang, and S. D. Bader, J. Magn. Magn. Mater. **200**, 392 (1999).
[37] A. Hoffmann, Phys. Rev. Lett. **93**, 097203 (2004).
[38] Y. J. Tang, D. J. Smith, B. L. Zink, F. Hellman, and A. E. Berkowitz, Phys. Rev. B **67**, 054408 (2003).
[39] S. Brems, D. Buntinx, K. Temst, C. Van Haesendonck, F. Radu, and H. Zabel, Phys. Rev. Lett. **95**, 157202 (2005).
[40] S. Soeya, T. Imagawa, K. Mitsuoka, and S. Narishige, J. Appl. Phys. **76**, 5356 (1994).